AD-A159 943 ADAPTIVE GRIDDING IN TWO DIMENSIONS FOR OPTIMAL ACCURACY AND EFFICIENCY(U) LAWRENCE LIVERMORE NATIONAL LAB CA E J KANSA 19 AUG 85 ARO-20585-1-MA 1/1

UNCLASSIFIED MIPR-ARO-124-84 F/G 12/1 NL

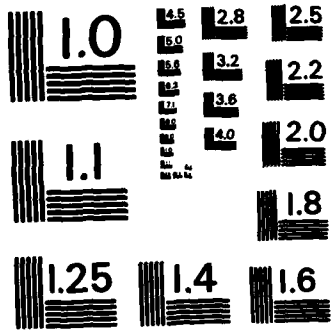

UNCLASSIFIED

SECURITY CLASSIFICATION OF THIS PAGE (When Data Entered)

AD-A159 943

REPORT DOCUMENTATION PAGE

READ INSTRUCTIONS BEFORE COMPLETING FORM

1. REPORT NUMBER: ARO 20585.1-MA
2. GOVT ACCESSION NO.: N/A
3. RECIPIENT'S CATALOG NUMBER: N/A

TITLE (and Subtitle)
Adaptive Gridding in Two Dimensions for Optimal Accuracy and Efficiency

5. TYPE OF REPORT & PERIOD COVERED: Mar. 1984 - Aug. 1985

6. PERFORMING ORG. REPORT NUMBER: Lawrence Livermore Natl Lab

AUTHOR(s)
Edward J. Kansa

8. CONTRACT OR GRANT NUMBER(s): MIPR-ARO-124-84

PERFORMING ORGANIZATION NAME AND ADDRESS
Lawrence Livermore National Laboratory, L-200
P O Box 808
Livermore, CA 94550

10. PROGRAM ELEMENT, PROJECT, TASK AREA & WORK UNIT NUMBERS

CONTROLLING OFFICE NAME AND ADDRESS
U. S. Army Research Office
Post Office Box 12211
Research Triangle Park, NC 27709

12. REPORT DATE: Aug. 19, 1985

13. NUMBER OF PAGES: 3

14. MONITORING AGENCY NAME & ADDRESS (if different from Controlling Office)

15. SECURITY CLASS. (of this report): Unclassified

15a. DECLASSIFICATION/DOWNGRADING SCHEDULE

16. DISTRIBUTION STATEMENT (of this Report)

Approved for public release; distribution unlimited.

17. DISTRIBUTION STATEMENT (of the abstract entered in Block 20, if different from Report)

NA

18. SUPPLEMENTARY NOTES

The view, opinions, and/or findings contained in this report are those of the author(s) and should not be construed as an official Department of the Army position, policy, or decision, unless so designated by other documentation.

19. KEY WORDS (Continue on reverse side if necessary and identify by block number)

Moving grid, one- and two-dimensional shock flow, mesh refinement, interacting shock waves, shock tracking, one-sided derivatives, consistent approximations, monotonic spline fits, no artificial viscosity, explicit calculations.

one and two dimensional

20. ABSTRACT (Continue on reverse side if necessary and identify by block number)

Very accurate 1 and 2-D shock calculations were made using moving grids, mesh refinements, consistent derivative formation, and Riemann solvers for interacting shocks. All calculations were done explicitly with no artificial viscosity. Error free 2D shocks were propagated using a grid velocity found by rotation into direction of the maximum gradient and subsequent translation on to a frame which appeared steady.

Add to keywords: Lagrangian Shock waves, Shock flow

DD FORM 1 JAN 73 1473 EDITION OF 1 NOV 65 IS OBSOLETE

UNCLASSIFIED

SECURITY CLASSIFICATION OF THIS PAGE (When Data Entered)

ARO 20585.1-MA

HIGHLY ACCURATE SHOCK FLOW CALCULATIONS WITH MOVING GRIDS AND MESH REFINEMENT

FINAL REPORT

Edward J. Kansa

August 19, 1985

U S ARMY RESEARCH OFFICE

Contract No. MIPR-ARO-124-84.

Lawrence Livermore National Laboratory

APPROVED FOR PUBLIC RELEASE;

Distribution Unlimited

A. Statement of Problem Studied

Contract No. MIPR-ARO 124-84 was a $35,000 grant to investigate methods for improving one and two dimensional shock flow calculations by combining several approaches such as mesh refinement and moving grids for optimal accuracy and efficiency.

B. Summary of Important Results

Extremely accurate shock flow results were obtained for standard one dimensional model problems. Inviscid hydrodynamics are piecewise continuous; derivatives at a discontinuity must be formed by appropriate one-sided difference approximations consistent with calculus. Because the spatial derivative at a discontinuity is unbounded, it can be made finite if the discontinuity is spread out using a consistent step function approximation, for example, an arctan. The derivative with the discontinuity is a finite approximation to a delta-function.

Second, a moving grid scheme was used. The grid velocity which is arbitrary is taken to be that velocity in which the set of dependent variables appear steady in the least squares sense. At a shock, contact surface or rarefaction, the grid velocity for each component was equal, but not necessarily equal in each continuous subregion. Wave steepening drives mesh points together and whenever the distance of closest approach fell below 0.0001 and the gradients in that region grew from successive time steps, a new discontinuity was inserted. A conservative static rezoning scheme was used as a post processor after every time step permitting grids to move without constraints.

After extensive testing, it was found that the standard local three finite difference scheme performed very poorly for derivative estimates in the rarefaction region. However, when a global monotonic spline interpolation developed by Fritsch and Carlson was used, vastly improved accuracy was obtained.

Mesh refinement was used for interacting shock waves in conjunction with a Riemann solver. The Riemann solver was used only to predict the outcome of a wave interaction, not to advance the solution in time. Mesh points were dynamically added to the computational domain for new shocks, contacts, and rarefaction waves. It was thus possible to follow the interaction of shocks with both step up and step-down contact interactions using a minimum number of points extremely accurately.

Finally a two dimensional freely propagating shock was calculated using the basic concepts developed in one-dimension. In 2D, the components of the grid velocity were found by rotation into the direction of the maximum gradient, and a translation to a frame in which the dependent variables are steady. Appropriate one sided differences were used at the shock. When standard stencils could not be used at or near the shock, a second order Taylor series on scattered data was used. The results for this problem were excellent.

Because of the limited contract grant, no mathematical analysis was done. The extension to the general case of 2D interacting shocks is unfinished, but the essential building blocks have been obtained. A superior method for differencing in two or three dimensions irregardless of a grid data structure appears to be Hardy's [1] multiquadric interpolation (MQI) scheme.

MQI is a locally global interpolation scheme which uses upper hyperboloids as basic functions. Franke [2] states that of all the methods he has tested MQI is outstanding in accuracy, visual appearance, ease of use, and timing. MQI is continuously differentiable permitting arbitrary data location without the dispersion and dissipation truncation errors associated with local low order interpolation based difference schemes. MQI has the power and accuracy of spectral methods without the restriction of a logically rectangular tensor product formulation.

Whenever possible, the analysis of Ben-Dor and Glass [3] and Mirels [4] will be used for the 2D regular and Mach reflection problem. However, the synthesis of the various aspects has yet to be done, and will be postponed until future funding.

Publication List

1. E. J. Kansa, "Highly Accurate Shock Flow Calculations with Moving Grids and Mesh Refinement", Proceedings of the 11th IMACS World Congress, Oslo, Norway, vol. 2, pp 89-92 (1985).

   The paper was presented on August 6, 1985 in Oslo in front of an audience of 70-80 people. Among the notables attending were: Burton Wendroff (LASL), Robert Warming (NASA-Ames), Douglas Dwoyar (NASA-Langley), Prof. David Pratt (Univ. Washington), Kenneth Marx (Chief Editor of Journal of Computational Physics and Sandia Laboratory), C. Albone, Royal Aircraft Establishment, UK., Prof. W. Schoenauer, Karlsruhe University, West Germany. These people personally congratulated me on my presentation and research work.

Bibliography

1. R. L. Hardy, "Multiquadric Equations of Topography and Other Irregular Surfaces", J. Geophys. Res., vol. 76, pp 1905-1915 (1971).

2. R. Franke, "Scattered Data Interpolation: Test of Some Methods", Math. Comp., vol. 38, pp 181-200.

3. G. Ben-Dor, "Regions and Transitions of Non Stationary Oblique Shock Wave Diffractions in Perfect and Imperfect Gases", UTIAS Report #232, Aug. 1978.

4. H. Mirels, "Mach Reflection Flow Fields Associated with Strong Shocks", AIAAJ, vol. 23, pp 522-529.

Proceedings of the 11th IMACS World Congress, Oslo, Norway, August, 1985; vol. 2, pp89-92.

Highly Accurate Shock Flow Calculations with Moving Grids and Mesh Refinement*

Edward J. Kansa
Lawrence Livermore National Laboratory
Earth Sciences Department, L-200
Post Office Box 808, Livermore, California 94550

Abstract

Five one-dimensional (1D) and one 2D shock wave problems which propagate obliquely to the coordinate axes are solved by a second-order time-marching method. The solution region is assumed to be piecewise continuous, with any "discontinuities" which may develop being represented by an arctan approximation to a step function. Immediately behind or ahead of a flagged "discontinuity", appropriate one-sided derivatives are used. An explicit moving grid technique is combined with the time-integration scheme which yields the correct velocity at "discontinuities". Shock fitting is not only simply handled, but it is handled automatically and correctly by the choice of the grid velocities. The regularization problem associated with moving grids is handled by a rezoning based on equidistributing the component averaged third derivative. Because the approximate step-function and the above-mentioned rules for derivative formation are mathematically consistent, artificial viscosity is unnecessary. The same second-order time integration scheme is used throughout the entire spatial domain. For accurate physics of wave interactions, a nonlinear Riemann solver is applied. In conjunction with the Riemann solver, adaptive mesh refinement injects mesh points into the computational domain automatically to define a post collision structure.

The Time-Marching Scheme

For brevity, the reader is referred to Richtmeyer and Morton [1] for details. The two-dimensional conservation law form of the fluid-dynamic equations is

$$\underline{U}_t + \underline{F}_x + \underline{G}_y = 0, \tag{1}$$

where the subscripts t, x, and y denote partial derivatives. The fluxes $\underline{F}$ and $\underline{G}$ are related to the conservative variables $\underline{U}$ in the following manner:

$$\underline{F}_x = \underline{A}\,\underline{U}_x; \quad \underline{G}_y = \underline{B}\,\underline{U}_y \tag{2}$$

where $\underline{A}$ and $\underline{B}$ are the appropriate Jacobians.

However, the matrix representation of the Jacobians can be ambiguous regarding the nonlinear matrix elements. The following procedure was used to guarantee rigorous equality. Given $\underline{F}_x$, $\underline{U}_x$, $\underline{G}_y$ and $\underline{U}_y$ as known quantities, the unknown nonlinear matrix elements of the Jacobians, $\underline{A}$ and $\underline{B}$ are solved.

The solution $\underline{U}$, at the new time t^{n+1} is given by a second order Taylor series expansion as

$$\underline{U}(n+1) = \underline{U}(n) - \int dt\,\{\underline{F}_x + \underline{G}_y\} + \tfrac{1}{2}\iint dt\,dt'\,\{[\underline{A}(\underline{F}_x + \underline{G}_y)]_x + [\underline{B}(\underline{F}_x + \underline{G}_y]_y\} \tag{3}$$

The Moving Grid Scheme

The approach taken in this paper is a modification of the simplified moving finite difference (MFD) scheme of Kansa et al. [2]. In that scheme, the penalty function approach for controlling grid motion was dropped in favor of a time step control and a static regridding scheme. The basic modification in this paper is that the grid velocities are part of an explicit time-integration scheme.

The conservation equations in a moving frame have the following form (relative to the fixed frame):

$$\underline{U}_t + (\underline{F}_x - v1\,\underline{U}_x) + (\underline{G}_y - v2\,\underline{U}_y) = 0, \quad dx/dt = v1,\ dy/dt = v2, \tag{4}$$

where the grid velocity, v, is arbitrary. In the absence of source terms, each PDE has a grid velocity for which a specific component of $\underline{U}$ is stationary which is chosen by

$$v1 = \underline{F}_x/U_x \text{ if } |U_x| \neq 0;\ v2 = G_y/U_y \text{ if } |U_y| \neq 0. \tag{5}$$

In special regions such as shocks, contact discontinuities, and rarefaction waves, all the component grid velocities are equal. For the convenience of dealing with a common grid, a common grid velocity was determined for the general case by requiring the entire set of dependent variables at a given location be stationary in the least-squares sense, [2]. The time-integration scheme, Eq. (3), is the same, except that the $\underline{A}$-matrix is now replaced by $\underline{A} - v\underline{I}$, and $\underline{F}_x$ is replaced by $\underline{F}_x - v\underline{U}_x$. In two dimensions, a rotation is performed which maximizes gradients along the prime coordinate, x'. Then a translation frame is sought in which $\underline{U}$ is stationary using Eq. (5).

Continuous Approximations of Discontinuities

Korn and Korn [3] have presented several approximate functions for the step function. The choice used in this paper approximates a step-function by the arctan function,

$$f(x) = \tfrac{1}{2}(f_r + f_\ell) + (f_r - f_\ell)/\cdot\arctan[s(x-x_o)]/\pi \tag{6a}$$

and $s = k/(x_r - x_\ell)$ for x in $[x_\ell, x_r]$ and where f_r and f_ℓ are the endpoint values of the discontinuity, x_o is the midpoint of the discontinuity, and s is the spreading parameter. Here the subscripts r and ℓ refer to the right (ahead) and left (behind) of a discontinuity moving to the right. In the limit of s going to infinity as $(x_r - x_\ell)$ goes to zero, f(x) becomes a true step function.

Three mesh points are sufficient to represent a "discontinuity": the two endpoints and the midpoint. Successive differentation of Eq. (6.a) yields the following midpoint derivatives:

$$f'(x_o) = (f_r - f_\ell)\,s/\pi \quad , f''(x_o) = 0\ . \tag{6b}$$

At the endpoints, the rules of calculus for piecewise continuous functions (see Korn and Korn [3]) are used to determine the derivatives at either side of a discontinuity.

* Work performed under the auspices of the U.S. Department of Energy by the Lawrence Livermore National Laboratory under contract No. W-7405-ENG-48 and partially supported by the Army Research Office contract No. MIPR-ARO 124-84.

$$f'(x_\ell) = f'(x_\ell^-); \quad f''(x_\ell) = f''(x_\ell^-) \tag{6c}$$

$$f'(x_r) = f'(x_r^+); \quad f''(x_r) = f''(x_r^+) \tag{6d}$$

Note that at the endpoints of a rarefaction fan, the function is continuous, but the derivatives are not. Eq. (6c) and (6d) are used at the appropriate locations.

Each component of $\underline{F}$ and $\underline{U}$ is fitted by its own step function at a "discontinuity". The grid velocity is found by using the appropriate flux and dependent variable derivatives, Eq. (6b) in Eq. (5). The entire "discontinuity" from x_ℓ to x_r moves at the grid velocity. Since one can store the appropriate derivatives, the same time-marching scheme, Eq. (3), can be used everywhere except at the boundary. Numerical experimentation has shown that in a moving frame, the first and second order terms of Eq. (3) are identically zero where the step function approximation is used. Using Eq. (6) in Eq. (3) and Eq. (4) requires no artificial dissipation. Shock fitting is automatically and correctly handled by this choice of moving grid velocities.

Because "discontinuities", corners of rarefaction fans, and boundaries are flagged, any shock flow can be partitioned into several distinct piecewise continuous subregions bounded by flagged and or boundary points. Grid motion in the subregions can be controlled by equipartitioning the component averaged third derivative, maintaining minimum spacing and well ordering of points, see [2]. The remapping is totally conservative because the integral of the old partition is forced to equal the integral of the new partition. In some circumstances, new discontinuities tend to develop.

The nonlinear convective terms of the governing PDE's permit steepening and eventual discontinuity formation. In a moving grid scheme, this phenomenon has been documented (see [2 and 4]). Given the current time step, grid positions, and velocities, a search is made within a piecewise continuous region to determine whether grid points would come within a separation of 10^{-4} or closer in the next time cycle, and if gradients are becoming very large. If so, a "discontinuity" defined by three points, see Eq. (6), is inserted into the computational domain, and another flag is set.

In this paper, a nonlinear 1-D Riemann solver is used to specify the physics of wave collisions. The Riemann solver is not used in any variations of the Gudunov scheme to time advance the solution. Therefore, it is instructive to outline the use of the Riemann solver in specifying the resulting physics after waves collide, such as shocks with rigid walls, geometric symmetry points, shocks with other shocks or contact surfaces, etc.

The Riemann solver will produce one of five possible middle state configurations depending upon input left and right state densities, velocities and pressures, located at X_ℓ and X_r. They are: (1) middle vacuum state, (2) a left and right rarefaction, (3) a left shock and right rarefaction, (4) a left and right shock, and (5) a left rarefaction and a right shock. If the middle left and middle right densities are unequal then a density discontinuity exists. Discontinuities and rarefactions are flagged.

Before advancing the solution and grid position to a new time, a search is made of all neighboring "discontinuities" using the relative separations and velocities to determine whether a wave collision is possible during the current time interval. If some collisions are possible, then the minimum collision time interval is found, and as a precaution, it is multiplied by 0.5.

If the separation of two existing waves is less than or equal to ϵ, where ϵ is arbitrarily chosen to be 10^{-3}, then the time interval to complete collision, Δt_1, can be calculated. Then the Riemann solver yields new states with new wave speeds. New discontinuities and rarefactions are flagged. The time interval, Δt_2, to the same separation can be calculated as well as the location within that separation of all the intermediate waves using the new wave velocities. Rather than fixing the total number of grid points, the number of grid points can be dynamically increased or decreased after the post collision states are determined.

Presentation of Results

Six example problems are presented. These are: the Riemann shock tube problem in cartesian geometry, the von Neumann spherical blast wave problem [5], the spherical blast wave problem of Noh [6], and the shock tube problem involving an interacting shock with a step-down and a step-up contact discontinuity. The last example is an infinite planar two-dimensional shock propagating obliquely to the coordinate axes.

All example calculations were solved in dimensionless form. The solutions have multiple time and length scales which evolve in time. The reference length scale is the distance from the origin at the left to the far right boundary, scaled to unity. The reference time scale is the reference length scale divided by the initial maximum speed. Relative to the initial length scale, the shock half width is arbitrarily chosen to be 10^{-4}.

The first case to be considered is the Riemann shock tube problem which was previously calculated by Sod [7] and Harten and Hyman [8] with the initial discontinuity at $x = 1/2$. At $t = 0$, a Riemann solver was used to initialize the solution at a time step Δt, on the domain $[0,1]$. A rarefaction wave propagates backwards while a shock, followed by a contact surface, propagates forward. This system has an analytic self-similar solution. The shock and contact surface propagate forward at constant velocities. The rarefaction fan propagates backwards along the local u-a characteristic, where u and a are the local particle and sound velocities.

Figure 1 shows the numerical solution for the density of $\gamma = 1.4$ gas at $t = 0.25$. The diamonds in these figures and all subsequent figures represent the actual solution at the indicated nodal position. Note that because the conservative variables (see Eq. 2) were used, the gas velocity and pressure at a discontinuity may not necessarily be the midpoint values.

The second problem attempted was the von Neumann [5] infinite shock, spherical blast wave problem. Ahead of the shock, $p = u = 0$ and $\rho = 1$. The pressure behind the shock at radius, $r = 1$, was specified to be 100. A special routine was used to initialize the solution behind the shock.

From the analysis of Zel'dovich et al. [9] and Thompson [10], the following relations can be obtained for a $\gamma = 5/3$ gas in terms of new variables:

$$\rho = 4\,\hat{\rho}, \; u = (r/t)\,\hat{u}, \; p = (r/t)^2\hat{p}. \tag{7}$$

Using the above relations in m and E as well as the fluxes, the following relation was observed:

$$\hat{U}_t + (1/t)(1/r^2)(r^2\,\hat{F})_r = 0. \tag{8}$$

Because of the (1/t) multiplying the flux transport terms, the integrating factor of Eq. (3) is $\ell n(t)$.

The results for pressure are shown in Fig. 2 at two different times. In the moving frame, only density is self-similar. The velocity and pressure profiles decay. The $\ell n(t)$ integrating factor gives the correct temporal behavior without unnecessarily small time steps.

The next problem to be discussed is Noh's [6] spherically divergent shock problem. At time $t = 0$, a $\gamma = 5/3$ gas at zero pressure, density of one, converges within a sphere at a gas velocity of -1. Then at the center, a shock develops with a density of 64, gas velocity of zero, and pressure of 64/3 moving outwards at a shock velocity of 1/3. Noh's challenge is to run the problem to a time of $t = 0.6$.

In order to solve the shock state due to the focusing of gas at the origin, the Riemann solver must be modified for infinite shocks and cylindrical and spherical geometry. As soon as the gas moves inward, it is adiabatically compressed by the spherical focusing. Since the initial pressure is zero, the subsequent pressure profile inward, but not at the origin is also zero. The inward gas motion

is self-similar with a constant gas velocity of u = -1, and the mass conservation equation can be integrated to yield

$$\rho = (1 + t/r)^2 \qquad (8)$$
$$\text{for } r>o$$

with the boundary condition

$$r = -t, \text{ at } \rho = 1 .$$

Because of spherical symmetry, the gas velocity must be zero at the origin. Using the notation that the subscripts ℓ and r refer to the left and right states ahead of the shock, and m to the new middle shock state, the known quantities are u_m, $p_\ell = p_r = 0$; $u_r = -1$, $u_\ell = 1$. The unknown quantities are P_m, ρ_m, $uS_r = -uS_\ell$, and $\rho_r = \rho_\ell$. Following Courant et al. [11], one finds for a $\gamma = 5/3$ gas that $\rho_r = 16$, $\rho_m = 64$, $us_r = 1/3$, and $p_m = 64/3$. Fig. 3 is the density calculated to t = 0.6. Note that the density has developed a new contact surface at the tail before it abruptly drops to unity. This discontinuity was inserted as discussed previously.

The next problem in slab geometry is adapted from Harlow and Amsden [12]. At t = 0, an incoming gas of velocity u = -1, p = 0 hits a rigid wall located at x = 0. The initial gas density is 2 for $x \leq 1/2$ and unity for $1/2 < x \leq 1$. The Riemann solver produces an outgoing shock moving at a velocity of 1/3 and an incoming contact discontinuity moving at a velocity of -1. Figure 4 shows the density, at t = 0.2 after the shock formation. Figure 4 also shows the density at t = 0.3169 just prior to the shock colliding with the contact discontinuity.

At the time of collision, the Riemann solver is used again, yielding a left traveling rarefaction, and a right traveling contact discontinuity and a shock with velocities 0.166 and 0.5547, respectively. The post collision states were resolved adequately by adaptive mesh refinement. Figure 4 also shows the density at t = 0.4184.

The fifth problem to be considered is also taken from Harlow and Amsden [12]. At t = 0, the initial state was defined to have a pressure equal to 10^{-4}, an incoming gas velocity of -1, and a density of 1 for $x \leq 1/2$ and 8/3 for $x < 1/2 \leq 1$. At x = 0, there is a rigid wall. A flow with a density jump hits a rigid wall, and a shock is formed. The shock proceeds to the right and collides with a step-up contact discontinuity. The Riemann solver, at the time of collision, gives as solutions a right and left traveling shock. Figure 5 shows the shock traveling at t = 0.2 to the right with a velocity $v_s = 0.333$ and a contact surface moving to the left at the velocity of -1. Figure 5 also shows the new states after collision at t = 0.31867. Although this appears to be an overshoot, the new states are spread over a distance of 0.001. The new state has two shocks, the left shock has a velocity of -0.909 and the right shock has a velocity of 0.0356. The middle contact has a velocity of -0.223.

Figure 6 shows the density at t = 0.4186 with left shock approaching the wall. At t = 0.463, Fig. 6 shows the density plot after wall collision. The shock hits the wall proceeding forward with a velocity of 0.7602. Figure 7 at t = 0.563 shows the density profile just prior to the collision of the contact with the left shock which reflected off the wall. Figure 7 also shows the profile after the shock from the wall collided with the contact at t = 0.703.

These calculations were extended at will without any evidence of difficulty. The calculations were arbitrarily stopped at t = 0.805. No instabilities have occurred because accurate solutions from the Riemann solver were used to define the collision states, a moving grid scheme was used, and a mathematically-consistent approximate step function was used without artificial viscosity. In this particular calculation, no CFL time restrictions were necessary since the first and second order time corrections (see Eq. 9.b) were identically zero. The time scale estimate used is $t = \|U\|/\|\nabla \cdot F - v \cdot \nabla U\|$. When the denominator vanishes, the time scale is arbitrarily large, however, the usual CFL condition is recovered when the grid motion is turned off.

The last problem is a demonstration that this moving grid scheme does indeed extend to higher dimensions. On a unit square, an infinite shock propagates obliquely to the coordinate axes. To the left of the shock for a $\gamma = 5/3$ ideal gas, p = 4/3, $\rho = 4$, u = v = 0; to the right of the shock, p = 0, $\rho = 1$, u = -1, v = - 5/8. The initial pressure profile is shown in Figure 8.

Two grids were used. An underlying coarse grid was used with $\Delta x = 1/6$ and $\Delta y = 1/5$. The shock region is defined on a mesh of length 7-11 grid points in the tangential direction and a width of 3 mesh points of total extent 10^{-4} in the normal direction. A two dimensional extension of a second order time marching scheme was used throughout the domain, except at the boundaries which were open. At the shock, a rotation was performed into the normal direction, and then a translational frame was found in which the conservative dependent variables were steady. The pressure profiles at t = 0 and t = 0.56 are shown. Note that the shock remains sharp. These calculations were run at a CFL number of 200. Figure 9 shows these results.

The future plans are to incorporate the two dimensional shock interaction analysis of Courant [11]. Because of the network of shock interactions, i.e., triple points, bubbles, etc. expected to arise from two dimensional interacting shocks, a rectangular mesh may become too cumbersome and scattered data interpolation schemes might be most useful.

References

1. R.D. Richtmeyer and K.W. Morton, "Difference Methods for Initial-Value Methods", Interscience Publ., 2nd Ed, NY (1967).
2. E.J. Kansa, D.L. Morgan, Jr., and L.K. Morris, SIAM J. Sci. Stat. Comput., vol 5, pp 667-683 (1984).
3. G.A. Korn and T.M. Korn, "Mathematical Handbook for Scientists and Engineers", 2nd Ed., McGraw-Hill Book Co., New York (1968).
4. J. Greenstadt, J. Comput. Phys., Vol. 53, pp. 299-318 (1984).
5. J. von Neumann, "John von Neumann, Collected Works", A.H. Taub, Vol. 6, pp. 219-237, The MacMillan Co., New York (1963).
6. W.F. Noh, UCRL-89623 (1983).
7. G.A. Sod, J. Comput. Phys., Vol. 27, pp. 1-31 (1978).
8. A. Harten and J.M. Hyman, J. Comput. Phys., Vol. 50, pp. 235-269 (1983)
9. Y.B. Zel'dovich and Y.P. Raizer, Editors, W.D. Hayes and R.F. Probstein, "Physics of Shock Waves and High Temperatue Hydrodynamic Phenomena", Academic Press, New York (1967).
10. P.A. Thompson, "Compressible Fluid Dynamics", McGraw Hill Book Co., New York (1967).
11. R. Courant and K.O. Friedrichs, "Supersonic Flow and Shock Waves", Interscience Publications, New York, N.Y. (1947).
12. F.H. Harlow and A.A. Amsden, "Fluid Dynamics", LA-4700, Los Alamos, New Mexico (1971).

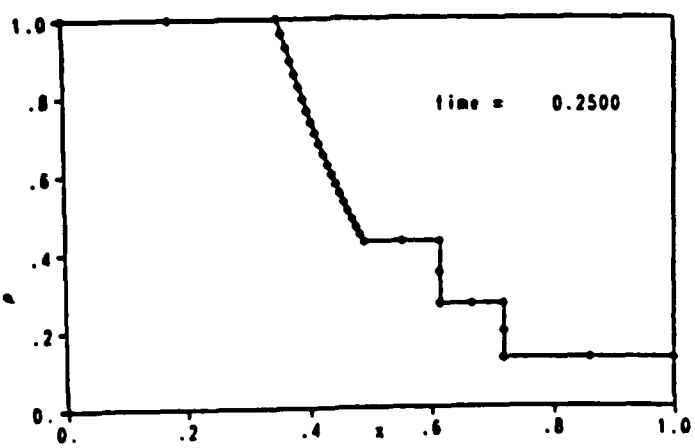

FIG.1 , RIEMANN SHOCK TUBE PROBLEM ,γ = 7/5

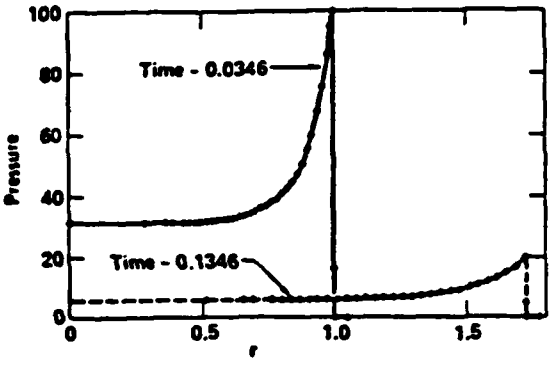

FIG.2, VON NEUMANN SPHERICAL BLAST WAVE, $\gamma = 5/3$

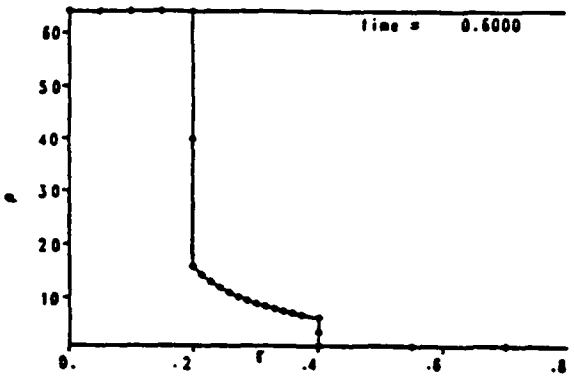

FIG.3, NOH'S SPHERICAL SHOCK WAVE, $\gamma = 5/3$

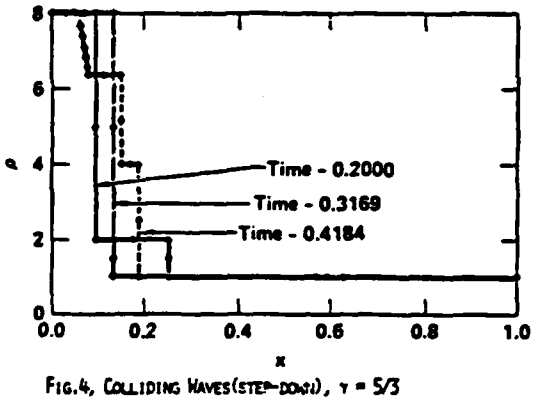

FIG.4, COLLIDING WAVES(STEP-DOWN), $\gamma = 5/3$

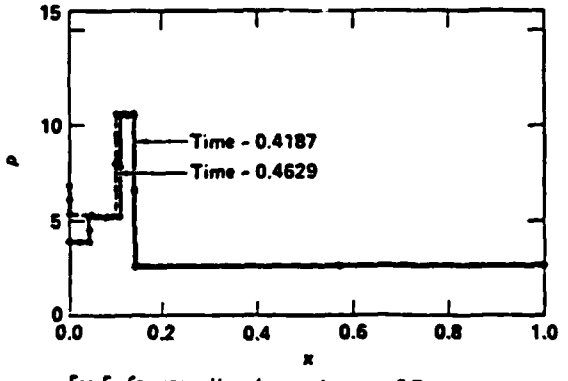

FIG.5, COLLIDING WAVES(STEP-UP), $\gamma = 5/3$

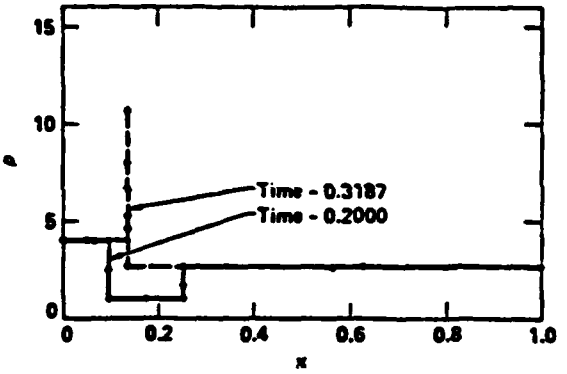

FIG.6, COLLIDING WAVES(STEP-UP), $\gamma = 5/3$

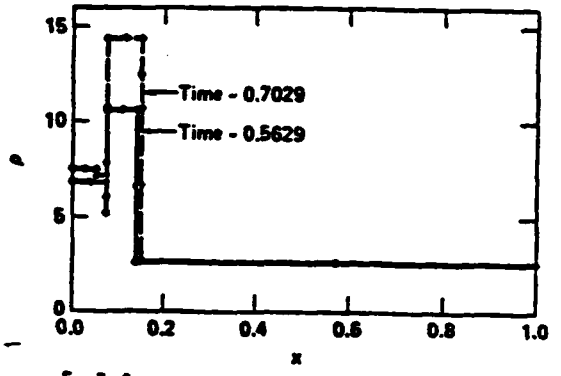

FIG.7, COLLIDING WAVES(STEP-UP), $\gamma = 5/3$

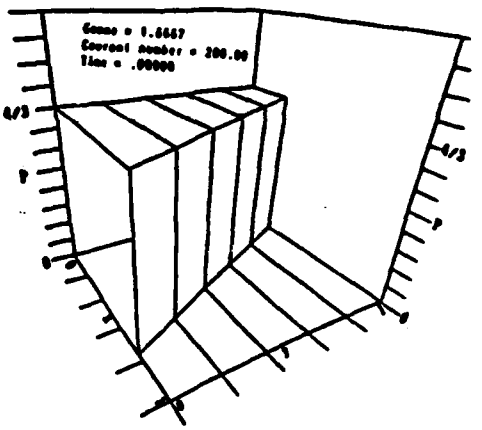

FIG.8, INFINITE 2D PLANAR SHOCK(INITIAL PROFILE), $\gamma = 5/3$

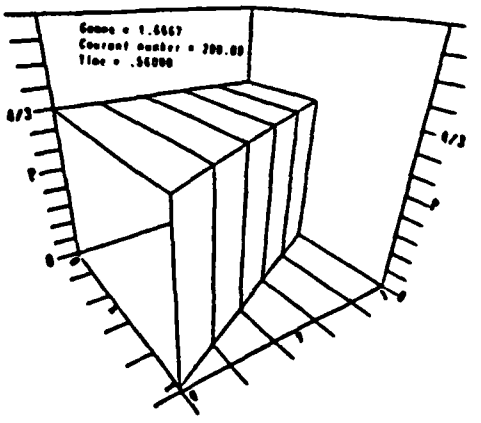

FIG.9, INFINITE 2D PLANAR SHOCK, $\gamma = 5/3$

END

FILMED

11-85

DTIC